Experimental aspects of cosmic rays

P. Sommers
University of Utah, Salt Lake City, UT 84112-0830, USA

Abstract
High-energy cosmic rays are detected as extensive air showers, and properties of the primary cosmic rays are deduced from measurements of those air showers. The physics of air showers is reviewed here in order to explain how the measurement techniques work. The Pierre Auger Cosmic Ray Observatory (near this school in Malargue) is used to illustrate the experimental methods. The Auger Observatory combines a surface array of water Cherenkov detectors with atmospheric fluorescence detectors. This 'hybrid' measurement technique provides high resolution and measurement cross-checks. In conjunction with a complementary site in the northern hemisphere, the Auger Observatory expects to map the arrival directions over the full sky as well as measuring the cosmic-ray energy spectrum and statistical properties of the mass distribution.

1 Introduction

A high-energy cosmic ray observatory records individual cosmic ray particles using the atmosphere as a transducer and amplifier. Each extremely high energy cosmic ray converts into a cascade that grows to billions of secondary particles. A large observatory records the air showers landing in a collection area that spans thousands of square kilometres. Because of the indirect measurement method, it is impossible to measure exactly the arrival direction, energy, and mass of the primary cosmic ray. Air shower measurements can determine the arrival direction to a small fraction of a degree. The energy, however, is hard to measure to better than 10% accuracy. The atomic mass of the primary particle cannot be estimated reliably for individual cosmic rays, and only some statistical properties of the primary mass distribution can be derived from air shower studies.

The flux of high-energy cosmic rays is tiny. Above 10^{19} eV, for example, the detection rate is approximately one per square kilometre per year. The rate falls by two orders of magnitude for each decade increase in particle energy. Direct measurement of the highest energy cosmic rays above the atmosphere is far from feasible. The study of extremely high energy cosmic rays must rely on indirect measurements via the air showers that those particles produce. Modern (hybrid) observatories combine a surface array of particle detectors with telescopes that observe radiation produced by the developing shower front as it traverses the atmosphere.

Physicists have used air showers to study cosmic rays near 10^{14} eV and above since Pierre Auger demonstrated the technique in 1938 [1]. The largest air-shower array, located near Malargue, is the Pierre Auger Observatory. It is designed for the study of the highest energy cosmic rays, making quality measurements of all air showers above 10^{19} eV that land within its 3000 km^2 area. Its surface detector (SD) is an array of 1600 water Cherenkov tanks. On good-weather nights, its air fluorescence detector (FD) measures the longitudinal development of the cascade as it descends through the atmosphere. The Auger Observatory will be used to illustrate the experimental techniques that are employed to measure the highest energy cosmic rays.

2 Air shower physics

An extremely high energy cosmic ray collides with a nucleus high in the atmosphere. The interaction produces many new energetic particles. Those also collide with air nuclei, and each collision adds a large number of particles to the developing cascade. Some of the produced particles are neutral pions,

each one of which immediately decays to a pair of gamma rays. The gamma rays produce $e^{\pm}$ pairs when passing near nuclei. The electrons and positrons re-generate gamma rays via bremsstrahlung, thereby building the electromagnetic cascade. This is an extensive air shower.

The number of charged particles in the air shower reaches a maximum size $N_{\rm max}$ that is nearly proportional to the primary energy E. There are billions of charged particles in high-energy air showers. The size $N_{\rm max}$ at shower maximum is approximately equal to E/1.5 GeV, although this conversion factor depends slightly on the choice of hadronic interaction model that is adopted to simulate collisions at energies above the reach of collider experiments, and it depends slightly on the atomic mass of the cosmic ray.

Experimental evidence so far indicates that extremely high energy cosmic rays are atomic nuclei (including protons which are hydrogen nuclei). The cosmic-ray nucleus initiates its air-shower cascade by hadronic interaction with an atomic nucleus in the atmosphere. The hadronic cascade (mostly pions) grows until the energy per pion falls to the level where pions are likely to decay before colliding. In each generation of the hadronic cascade, 1/3 of the energy on average goes to neutral pions which instantly decay to pairs of gamma rays. Each gamma ray develops an electromagnetic subcascade. After n hadronic cascade generations, only $(2/3)^n$ of the total energy remains in the hadronic cascade.

The decay of π^0 mesons into gamma rays eventually transfers most of the primary cosmic ray's energy to the electromagnetic cascade. Each gamma ray converts to an $e^{\pm}$ pair. The electrons and positrons create new gamma rays by bremsstrahlung. The radiation length $X_{\rm r}$ is the grammage path length in which their energies attenuate by the factor $1/e$. In air, this radiation length $X_{\rm r}$ is 36.2 g/cm^2. The electromagnetic cascade grows via pair production and bremsstrahlung.

Heitler's heuristic picture [2] of the electromagnetic cascade gives intuitive understanding of its essential properties. One imagines the cascade developing by a sequence of generations. At each generation, any gamma ray produces an $e^{\pm}$ pair, while each electron or positron produces a gamma ray in addition to itself. Every generation therefore doubles the number of cascade particles. The grammage interval for each generation is $X_{\rm r}\times$ ln(2), i.e., the path over which the energy of any one particle is expected to be reduced by 1/2. The process continues until the average particle energy is reduced to the *critical energy* below which charged particles lose their energy in less than one radiation length by ionizing atoms. Given that the ionization energy loss is about 2.2 MeV/g/cm^2, the critical energy $E_{\rm c}$ is (2.2 MeV/g/cm^2)$\times$(36.2 g/cm^2) = 80 MeV. The cascade grows until it reaches size $N_{\rm max} = E/E_{\rm c}$. The number of generations n needed to reach this maximum size depends on the total energy E. Since the number of particles doubles at each generation, one has at maximum, $N_{\rm max} = 2^n = E/E_{\rm c}$, so $n = \ln(E/E_{\rm c})/\ln(2)$. The maximum size occurs at a slant depth $X_{\rm max} = n \times X_{\rm r} \times \ln(2) = X_{\rm r} \times \ln(E/E_{\rm c})$ (measured along the shower axis from the top of the atmosphere).

Rigorous treatments show that this heuristic model gives the correct depth of maximum ($X_{\rm max}$) for each energy. In particular, the depth of maximum $X_{\rm max}$ for electromagnetic cascades increases by $X_{\rm r}\times$ ln(10) for each decade of increase in energy E. This *elongation rate* of 85 g/cm^2/decade is greater than what is expected for air showers that are fed by hadronic cascades.

The heuristic model's suggestion that $N_{\rm max}$ is proportional to energy is only approximately true. The total energy is equal to 2.2 MeV times the charged particle shower size integrated over all depths, as the electromagnetic energy is dissipated by charged particles at the rate of 2.2 MeV/g/cm^2/particle. Because the *longitudinal profile* $N_{\rm e}(X)$ gets longer ($X_{\rm max}$ larger) with energy, the height of the profile curve cannot be strictly proportional to energy. In fact, $N_{\rm max} \propto E/\sqrt{\ln(E)}$. To a good approximation, this is proportional to E in accordance with the heuristic model.

Rigorous treatments show that the electromagnetic longitudinal profile is accurately given by the Greisen formula [3]:

$$N_{\rm e} = \frac{0.31}{\sqrt{T_{\rm max}}}\, e^T\, s^{-3T/2}\,.$$

Here T is the atmospheric depth measured in radiation lengths ($T = X/X_{\rm r}$) from the point of the gamma ray's production, $T_{\rm max} \equiv \ln(E/E_{\rm c})$, and s is the *shower age*: $s \equiv 3T/(T + 2T_{\rm max})$. Many shower properties are well parametrized by shower age. All positive values of atmospheric depth occur in the range $0 < s < 3$, and shower maximum occurs at shower age $s = 1$.

In the hadronic cascade, the charged pions produce air shower muons when they decay. The number of shower muons depends on the amount of energy that is left in the hadronic cascade when pion energies have dropped to the level where decay is more likely than collision. If this happens after relatively few cascade generations, then copious muon production occurs. If the reduction of pion energies takes relatively many generations, then more of the energy will have been lost from the hadronic cascade to the electromagnetic cascade, and meager muon production occurs.

A cascade initiated by an iron nucleus develops like a superposition of 56 nucleons, each with 1/56 of the primary energy. In effect, this jump-starts the cascade, and pions get down to energies where they can decay to muons before the electromagnetic cascade has drained too much energy from the hadronic cascade. An iron shower therefore typically has more muons than a proton shower of the same total energy. Moreover, the superposition of 56 lower energy subshowers reaches its maximum size higher in the atmosphere than a proton shower of the same total energy. Statistical determinations of the primary mass distribution (chemical composition) exploit these differences between heavy and light nuclei: heavy nucleus showers produce more muons and they reach maximum size higher in the atmosphere.

The longitudinal development (rise and fall of the number of charged particles) is frequently approximated by a parametrized Gaisser–Hillas functional form [4]:

$$N_{\rm e}(x) = N_{\rm max}\,(\frac{x}{w})^{w}\,e^{w-x}\,,$$

where $w \equiv (X_{\rm max} - X_0)/\lambda$, $x \equiv (X - X_0)/\lambda$, and λ is an interaction scale length in g/cm^2. The four parameters ($N_{\rm max}$, $X_{\rm max}$, X_0, λ) provide ample size and shape freedom for fitting longitudinal profiles. As an exercise, try fitting the Greisen function (given above) by a Gaisser–Hillas function with appropriate choice of parameters.

3 Geometric reconstruction

Surface arrays determine the arrival direction by recording the arrival time of the shower front at three or more non-collinear stations on the ground. The method is conceptually simple assuming the shower front to be a perfect plane. Any pair of stations A and B determine the arrival direction cosine along the direction from A to B as $c(t_{\rm A} - t_{\rm B})/\bar{\rm AB}$, where c is the speed of light, $t_{\rm A}$ and $t_{\rm B}$ are the trigger times for stations A and B, respectively, and $\bar{\rm AB}$ is the distance between them. Two independent direction cosines determine a unique arrival direction in the hemisphere above the plane of the detectors.

The shower front is actually a curved surface, not a plane. The trigger times of three or more stations give the geometry by chi-square minimization, using the expected relative arrival times based on a realistic curved shower front moving at the speed of light. Those expected times depend not only on the arrival direction but also on the core position, so the core should first be determined from the relative station signal amplitudes.

Geometric reconstruction is quite different for a fluorescence detector eye, which sees an air shower as a spot of light that moves downward through the atmosphere at the speed of light. The track of the spot's centre defines a great circle in the direction space of the eye which, together with the eye's location, determines the shower-detector plane (SDP). If two eyes at different locations record the same shower, then the shower axis must lie in both SDPs. The intersection of the planes determines the shower axis (provided the two planes are not the same). This is the *stereo* reconstruction method. The angular resolution depends on the accuracy of determining the SDPs and on the opening angle between them. The SDP accuracy is better for longer tracks and smaller pixels [5].

Data from a single FD eye together with the trigger time(s) from one or more SD stations yield a hybrid geometric reconstruction that offers better accuracy than stereo reconstruction. After determining the SDP, 'geometric reconstruction' means identifying the shower axis within the SDP together with the time when the shower front passes some point on that axis. To understand the hybrid method, imagine that you know precisely the angular velocity of the track as the spot passes the centre of some particular pixel. If somebody were to tell you the distance to the shower axis at that point of the track, you could calculate when the light was emitted from that point of the axis and (using the measured angular velocity) what angle the axis makes with the pixel's viewing direction. The geometric reconstruction is therefore complete if you are told that one distance to the axis. Since you may not know it accurately from the FD data alone, you can try all possible distance hypotheses. Each one gives a unique geometric reconstruction and therefore a unique prediction for the trigger time of any SD station on the ground. The trigger time of any ground station therefore identifies which distance hypothesis is correct and therefore the true geometry. This timing method typically picks out the axis within the SDP with less uncertainty than if the axis is determined by a second (stereoscopic) SDP. For stereo hybrid events, there are timing determinations in two independent planes, providing reconstruction accuracy that is superior to both stereo reconstruction and monocular hybrid reconstruction.

4 Energy measurement

Conceptually, energy determination by a fluorescence detector is straightforward. The amount of emitted fluorescence light is proportional to the ionization energy loss by all the charged particles. Measuring the fluorescence emission from the full shower development should yield the total electromagnetic shower energy. It is a robust calorimetric measurement. The only dependence on hadronic model or composition is in the small fraction of primary energy that is assumed to escape the hadronic cascade as muons and neutrinos rather than being transferred to the electromagnetic cascade. Simulations suggest that this fraction is approximately 5% for proton showers and 15% for iron showers. By assuming 10%, the error due to ignorance of the primary particle should not be more than about 5%. Still, it is important to recognize that air shower measurements are an indirect method for determining the energy of a cosmic ray, and there is *some* systematic model uncertainty that is difficult to quantify. The fraction of the cosmic ray energy not dissipated electromagnetically also fluctuates shower-to-shower, especially for protons.

Implementing this conceptually simple calorimetric method encounters numerous difficulties:

1. The full longitudinal development is never observed. The FD records only the portion of the shower development that is above ground level and large enough to produce a detectable light flux at the detector. Some extrapolation using a fitted functional form is needed to account for the parts of the development that are not measured.
2. Light scattered to the FD from the intense forward Cherenkov beam contaminates the fluorescence signal. This scattered Cherenkov light distorts the spectrum of detected photons as well as their number.
3. The optical clarity of the atmosphere is variable because of changes in the aerosol density and aerosol composition. This makes it problematic to infer the amount of emitted light based on the observed flux. Detailed atmospheric monitoring can, in principle, overcome this difficulty.
4. The fluorescence efficiency is not precisely known. The number of fluorescence photons produced per metre along a charged particle's trajectory depends on the particle's energy and also on the atmospheric temperature and pressure where the particle is. Uncertainty in the fluorescence efficiency causes uncertainty in inferring energy deposition based on the amount of produced fluorescence light.

Numerous laboratory experiments are tackling the last itemized difficulty [6], and they can be expected to reduce the uncertainty in cosmic-ray energy measurements which is due to uncertainty in the fluorescence yield. The other difficulties introduce energy errors that are more random than systematic.

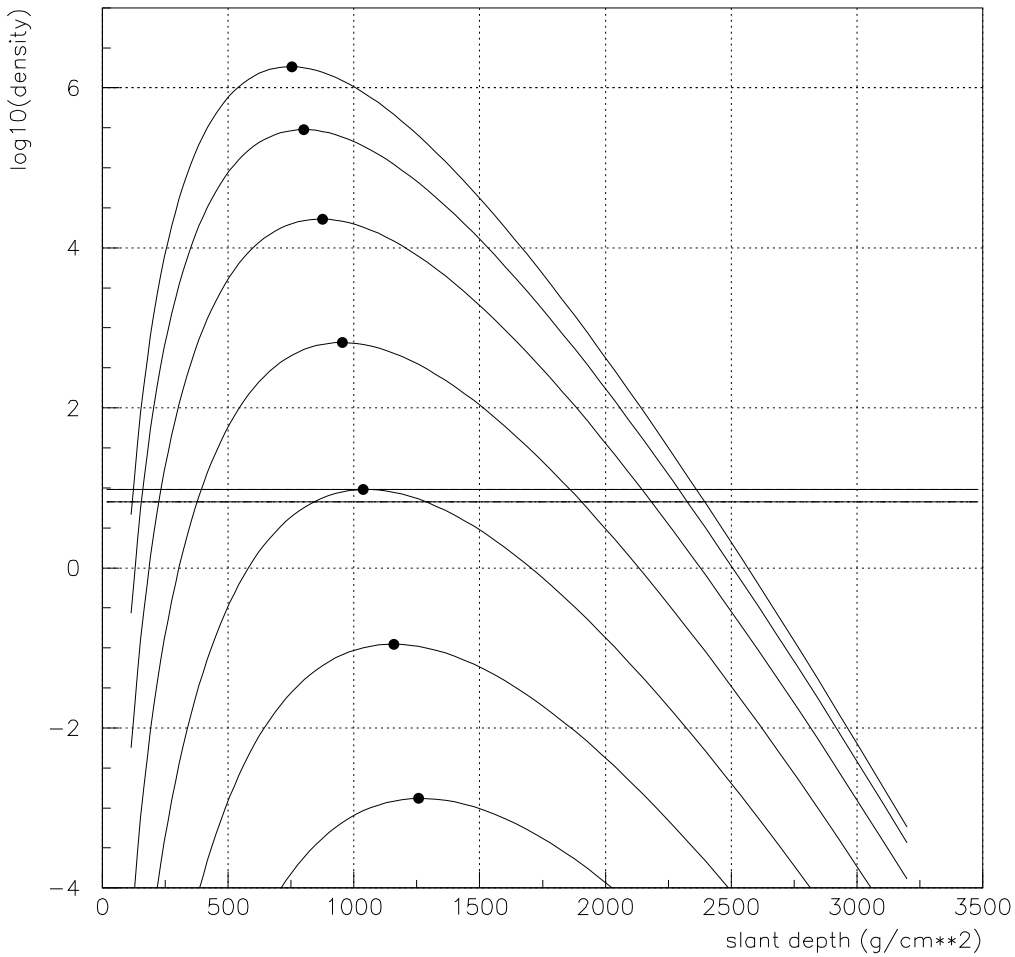

Fig. 1: Longitudinal development curves for the NKG electromagnetic particle density at seven fixed distances from the shower axis. The distances are fixed in Molière units but converted to metres using the Auger detector altitude. Top to bottom, the distances (in surface metres) to the axis are 10, 32, 100, 320, 1000, 3200, 10 000. Note that the depth of maximum increases with distance from the axis. Two horizontal lines mark the maximum of s_{1000} curve and the value 30% lower. The density remains within 30% of its maximum from 850 to 1300 g/cm^2. The units are approximate number of vertical equivalent muons per 10 m^2 for this shower of $N_{\rm max} = 6 \times 10^9$.

The FD quasi-calorimetric energy measurement can provide an important calibration for SD energy measurements which otherwise rely on shower simulations. Shower simulations are necessarily uncertain in their treatment of hadronic interactions at energies that have not been studied by collider experiments.

Simulations show that the signal collected in SD stations far from the core is approximately proportional to the total shower energy. In the case of the Auger array, the signal (s_{1000}) deposited in a water tank 1000 meters from the core is taken to be proportional to shower energy. At that distance, the longitudinal development of particle density reaches its maximum value near ground level for a large range of zenith angles. Since a smooth function changes very little near its maximum value, this method is relatively insensitive to fluctuations in shower development.

Figure 1 shows the longitudinal development profiles for the particle density at seven different distances from the shower axis. The curves are analytic: the total shower size as a function of depth is taken to be a Gaisser–Hillas development curve and the lateral distribution at each depth (hence shower

age) is given by the NKG function [7, 8]:

$$\rho(r) = \frac{N(s)}{R_{\rm M}^2}\, r^{s-2}\, (1+r)^{s-4.5} \,/\, [2\pi B(s, 4.5-2s)]\,,$$

where $N(s)$ is the number of charged particles at age s and $B(x,y) \equiv \Gamma(x)\Gamma(y)/\Gamma(x+y)$ is the standard 'beta function'. The different curves correspond to different fixed distances from the axis measured in Molière units, using the single conversion to metres that pertains at the Auger ground level. Each density longitudinal profile has a dot indicating its maximum. You can see that the depth of maximum increases with Molière distance from the core. Although the total shower size reaches maximum at 800 g/cm^2 in this example, the density s_{1000} (measured at the Molière radius that corresponds to one kilometre at ground level) reaches maximum at more than 1000 g/cm^2. A detector at vertical depth 850 g/cm^2 (Auger) or 920 g/cm^2 (AGASA) is therefore well positioned to be near the s_{1000} maximum for zenith angles at least up to 45 degrees. The horizontal dashed lines in the figure mark the maximum of the s_{1000} curve and the value that is 30% less. You can also see that the density stays within 30% of its maximum from 850 g/cm^2 to 1300 g/cm^2. Fluctuations in shower development (and even the systematic difference between protons and iron) shift the maximum by only about 100 g/cm^2 or less.

Knowing the slant depth of a shower's measurement, the expected longitudinal development profile of s_{1000} allows one to correct the measured s_{1000} to what it likely was at maximum. For large zenith angles, these correction factors become dangerously large for scintillator arrays. For water Cherenkov detectors, the longitudinal profiles fall much slower with slant depth than the (electromagnetic) NKG behaviour plotted in Fig. 1. For water Cherenkov arrays, therefore, relatively small corrections to s_{1000} are needed even at large zenith angles to give the ground parameter (s_{1000} at its maximum), which is proportional to energy.

None of the triggered ground stations is likely to be exactly 1000 metres from the axis. Interpolation using numerous stations closer to and farther from the axis gives the estimate for the signal density at 1000 m. Rather than using linear interpolation, one fits an empirical average lateral distribution functional form and takes as s_{1000} the value of that fitted function at 1000 metres from the axis.

A statistical correlation of s_{1000} with shower energy measured calorimetrically by the FD yields the conversion factor from s_{1000} to energy without relying on shower simulations that use untested hadronic interaction models. A large hybrid data set will determine the conversion factor's dependence on zenith angle.

5 Composition analysis

The indirect measurement of a cosmic ray by its air shower makes it impossible to measure the mass of the primary particle exactly. Shower-to-shower fluctuations in longitudinal development can make an air shower produced by a particle of one mass indistinguishable from an air shower initiated by a particle of a different mass. As described in Section 2, however, each mass value leads to its own expected value for the shower depth of maximum and number of muons (at each energy). These quantities are both intimately related to the speed of shower development, but fluctuations in $X_{\rm max}$ are not highly correlated with fluctuations in N_μ. For example, a fluctuation in depth of first interaction relates directly to a shower's $X_{\rm max}$, but it has little impact on the shower's N_μ. Direct or indirect measurements of $X_{\rm max}$ and/or N_μ provide important information about the primary mass distribution, even though it is not feasible to determine the masses of individual primary cosmic rays.

The 'superposition model' is a useful approximation that is remarkably accurate (although not exactly correct). Its premise is that *an air shower by a nucleus (E,A) behaves like the superposition of A proton showers, each with energy E/A*. (Note that this is not the same as supposing that it breaks into *A* nucleons at its first interaction.) The expected difference between proton and iron air showers of a given energy can be evaluated simply using this superposition model. Their difference in $X_{\rm max}$ and number of muons N_μ will be considered here.

Denoting the expected value of $X_{\rm max}$ by $\bar{X}_{\rm max}$, the difference between proton and iron at fixed energy E is given by

$$\bar{X}^{\rm P}_{\rm max}(E) - \bar{X}^{\rm Fe}_{\rm max}(E) = \bar{X}^{\rm P}_{\rm max}(E) - \bar{X}^{\rm P}_{\rm max}(E/56) = ER \times {\rm Log}(56) \; .$$

Here ER is the proton elongation rate (change in $X_{\rm max}$ per decade change in energy). Taking $ER \sim 57$ g/cm^2/decade implies that proton air showers are expected to reach maximum development approximately 100 g/cm^2 deeper in the atmosphere than iron showers of the same total energy.

To evaluate the difference in muon content N_μ one assumes a power-law dependence of $\bar{N}_\mu$ on energy for proton showers: $\bar{N}_\mu(E) = \alpha E^\beta$. For this argument, this power-law dependence only needs to be a good approximation over an energy range $E/56$ to E for the energy of interest. With this assumption, then,

$$\bar{N}^{\rm Fe}_\mu(E) = 56\bar{N}^{\rm P}_\mu(E/56) = 56\alpha(E/56)^\beta = 56^{1-\beta}\alpha E^\beta = 56^{1-\beta}\bar{N}^{\rm P}_\mu(E) \; .$$

Therefore,

$$\bar{N}^{\rm Fe}_\mu(E)/\bar{N}^{\rm P}_\mu(E) = 56^{1-\beta} \; .$$

At energies near 10^{19} eV, $\beta \approx 0.93$, so this ratio is approximately 1.3. Iron showers are expected to have 30% more muons than proton showers of the same total energy.

A surface detector measures shower parameters that are sensitive to $X_{\rm max}$. These include the lateral steepness and the shower front curvature. A shower whose maximum is farther above the surface has a flatter lateral distribution and less curvature in its shower front. The shape of the detector signal pulses can be sensitive to the relative contribution from muons. Muons suffer less Coulomb scattering and arrive more promptly than electromagnetic particles. A shower by a heavy nucleus (like iron) is expected to produce signal pulses that rise and fall rapidly relative to pulses in showers produced by light nuclei (like protons). Cronin [9] has therefore advocated studying composition by the distribution of the 'shape parameter' of signal pulses in water Cherenkov detectors at a distance of 1000 metres from the core. The suggested parameter is the ratio of signal accumulated in the first 600 ns to signal collected after the first 600 ns. Heavy primaries are indicated by large values of the shape parameter and light primaries by small values.

Fluorescence detectors can measure $X_{\rm max}$ directly. Analyses of the mean $X_{\rm max}$ as a function of energy in Fly's Eye [10] and HiRes [11, 12] data have suggested that the composition gets significantly lighter with energy near or before the spectrum's ankle.

A hybrid data set has special value in studying the cosmic ray chemical composition. The FD measures the electromagnetic shower energy and the depth of maximum $X_{\rm max}$. Water Cherenkov detectors are sensitive to the muon composition. At any fixed electromagnetic energy, heavy and light components can be separated when s_{1000} is plotted versus $X_{\rm max}$, as shown in Fig. 2 [13].

Combining also a scintillator array with a water Cherenkov array and fluorescence detectors should allow an even more powerful probe of the primary mass distribution. The scintillator array is sensitive to the surface electromagnetic particle density, allowing that to be subtracted from the water Cherenkov signal to measure the contribution due to muons.

Determining the primary mass distribution is challenging because of the indirect method of measuring cosmic rays by their air showers. There are many measurable parameters that correlate with the primary mass, however. These include the depth of shower maximum $X_{\rm max}$, the shower front curvature, the signal rise times, and the steepness of the lateral distribution. Multi-parameter analyses may provide the best sensitivity. Neural networks are a special kind of multiparameter analysis. A neural net can provide a mass likelihood distribution for each measured shower, based on its multiparameter training with simulated showers.

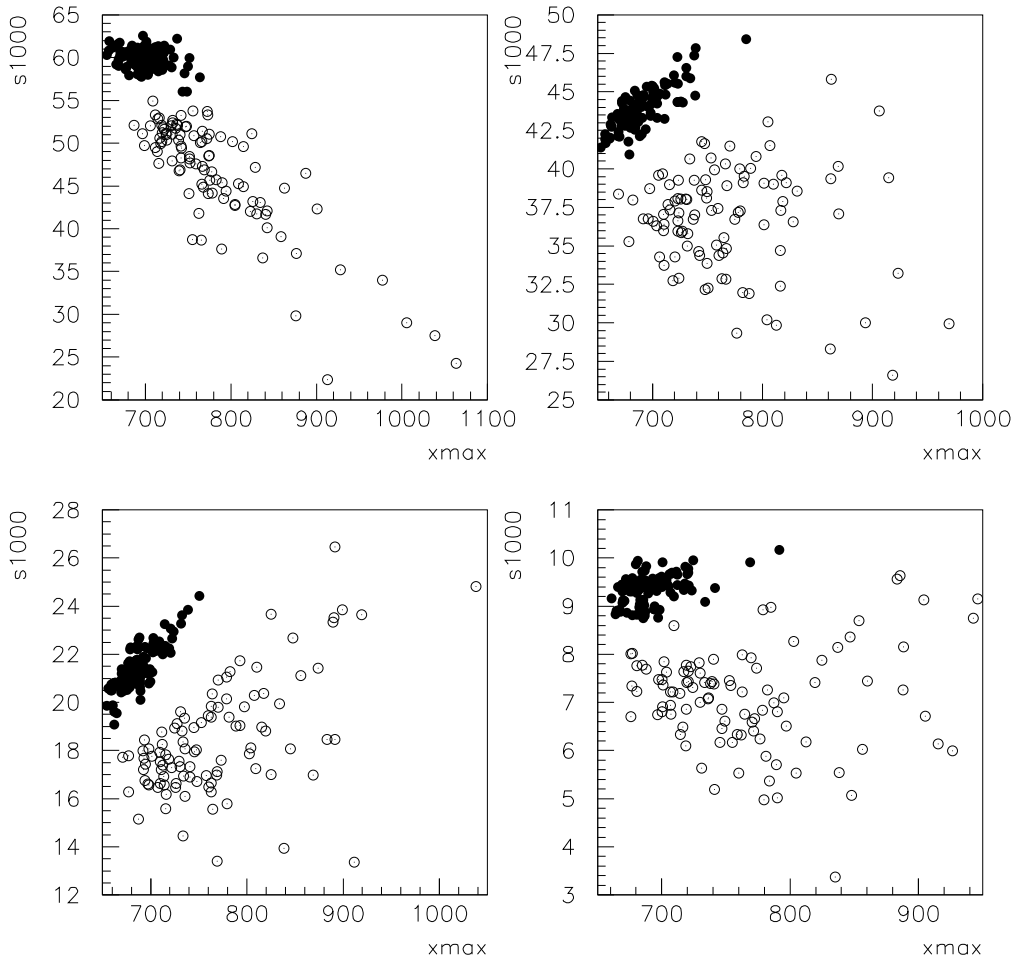

Fig. 2: Proton showers (○) are separated from iron showers (●) in this scatter plot of s_{1000} vs. $X_{\rm max}$. These are simulated showers of 10^{19} eV at zenith angles of 0, 37, 53, and 66 degrees, using CORSIKA and QGSJET.

6 Identifying photon primaries

Extremely high energy gamma-ray primary particles produce electromagnetic air showers that differ significantly from those produced by primary nuclei. Some muons occur by virtue of pion photoproduction, but the number of muons is an order of magnitude less than in showers initiated by primary hadrons. Moreover, the depth of maximum is expected to be greater for a gamma-ray primary than for a primary hadron. Recall that the 'elongation rate' for electromagnetic showers is 85 g/cm^2/decade, whereas it is only about 57 g/cm^2/decade for protons. (High-multiplicity hadronic interactions serve to divide the primary energy faster than the electromagnetic pair-production and bremsstrahlung processes.) Although proton showers develop similarly to gamma-ray showers at much lower energies, the proton showers develop significantly faster near 10^{19} eV and above.

The techniques for studying chemical composition using direct or indirect measures of $X_{\rm max}$ or muon content are able to detect the existence or not of a component of gamma rays in the extremely high energy cosmic rays. The Cronin shape parameter, shower front curvature, lateral steepness, and direct measurement of $X_{\rm max}$ should all be able to identify gamma-ray primaries if they are present in the cosmic ray flux. Some models for cosmic ray production (especially the 'top-down' models in which the cosmic rays result from the decays of supermassive particles) predict a dominant (or at least

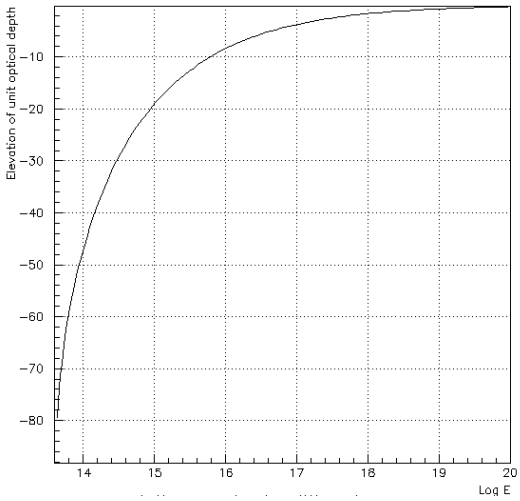

Fig. 3: The elevation angle (negative) which corresponds to optical depth of 1 for neutrinos coming through the Earth as a function of neutrino energy. The Earth is nearly opaque above 10^{17} eV.

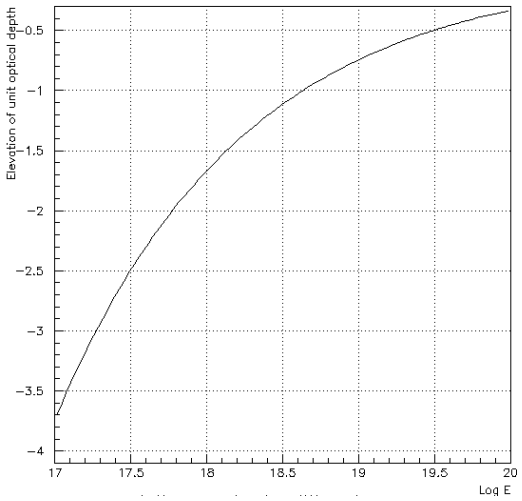

Fig. 4: Detail of the left figure for energy greater than 10^{17} eV. Above 10^{18} eV, the neutrinos must only skim the Earth at an upward angle less than 2 degrees from horizontal.

significant) component of primary gamma rays at extremely high energy. The absence of a clear gamma-ray component would rule out many such scenarios.

Above 10^{19} eV, two other effects introduce a different signature of a gamma-ray component. One effect is the Landau–Pomeranchuk–Migdal (LPM) effect [14], which decreases the electromagnetic cross sections and consequently lengthens the electromagnetic shower development. The other effect is magnetic pair production in the Earth's magnetosphere [15]. A superhigh-energy gamma ray crossing magnetic field lines can produce an $e^{\pm}$ pair. Those will synchrotron-radiate in the magnetic field, producing additional high-energy gamma rays. A different kind of electromagnetic cascade develops in the magnetosphere, but the effect is similar to adding some radiation lengths above the atmosphere. The important thing is that this occurs only if the primary gamma ray arrives transverse to the geomagnetic field. If it arrives approximately parallel to field lines, then there is no 'pre-showering'. Gamma rays arriving transverse to field lines cascade to lower energy particles above the atmosphere and are little affected by the LPM effect. Their atmospheric longitudinal developments are shortened by their head-start in the magnetosphere. In contrast, those same gamma rays arriving parallel to the magnetic field lines would get the full LPM effect and have stretched-out shower developments. Looking at shower development speed as a function of arrival direction relative to the local magnetic field direction is a way to look for evidence (or not) of gamma rays at the highest energies.

7 Neutrino detection

A giant cosmic-ray observatory like Auger makes an effective neutrino observatory at EeV energies. The detection is especially efficient for tau neutrinos, so it is fortunate that neutrino mixing makes tau neutrinos approximately as abundant as the other flavours for astrophysical high-energy neutrinos. An EeV tauon lives long enough to travel 50 km, on average. A tauon produced in the ground with a trajectory of small elevation angle will decay into showering particles above the surface array, and the air shower will be sampled by the particle detectors. The signature of a young (small age) electromagnetic shower is clearly distinguishable from a (very old) near-horizontal shower produced by a normal cosmic ray. The shower front curvature is much smaller, and the individual detector flash-analog-to-digital converter (FADC) traces are much broader.

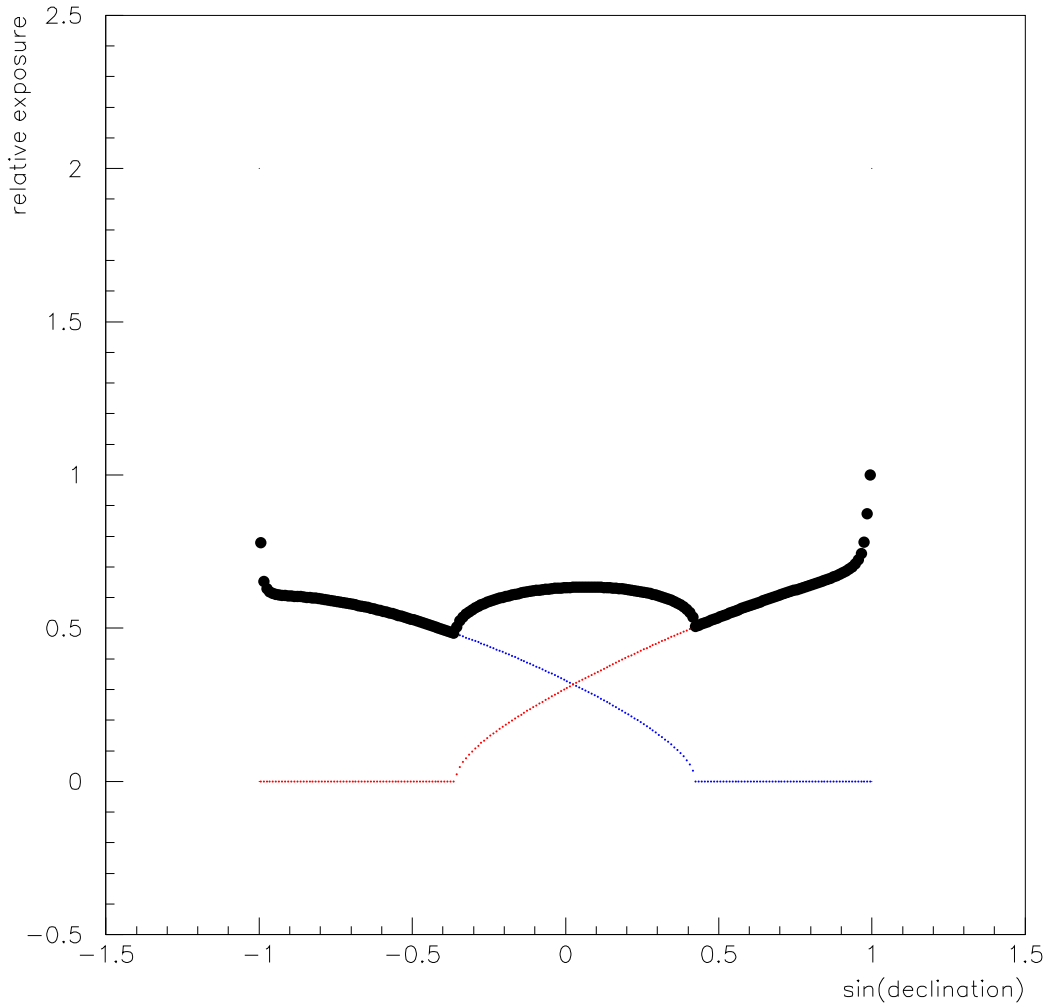

Fig. 5: The exposure versus celestial declination. This is for an observatory array with acceptance out to 60 degrees in zenith angle. The southern site is assumed to be at latitude –35 degrees and the northern site at +39 degrees.

The Earth is opaque to neutrinos at EeV energies and above, as shown in Figs. 3 and 4. This means that detectable neutrinos must come from near-horizontal 'Earth-skimming' directions, so that the total grammage of their trajectory in the Earth is not too large. This does not reduce the Auger aperture (as it does for detectors like IceCube) because Auger can only detect and distinguish air showers resulting from neutrino interactions if they are nearly horizontal. Auger should be able to detect some neutrinos arising from the GZK pion photoproduction process [16]. The magnitude of this neutrino flux at EeV energies is an important handle on the production and propagation of the highest energy cosmic rays.

8 Anisotropy analysis

The search for the sources of high-energy cosmic rays requires measuring more than their energy spectrum and composition. Those do not adequately constrain the possible theories. Whatever spectrum and composition might be measured, theorists would find multiple models for the origin of cosmic rays that are compatible with those results. An anisotropy fingerprint is needed to identify the sources definitively. This is true whether the sources are resolved as discrete spots on the sky or whether their signature is a large-scale pattern.

The Auger Observatory was designed to detect cosmic rays with almost uniform sensitivity over the entire celestial sphere. Because the Earth is opaque to cosmic rays (and rotates only about one axis), full-sky exposure requires detectors in both the northern and southern hemispheres. Figure 5 shows that the southern site by itself is blind to 1/4 of the sky, and there is a steep gradient over half of the remainder. Similarly, the northern site is blind to the 1/4 of the sky that the southern site sees well, and its gradient is opposite that of the southern site in the 1/2 of the sky where they overlap. Their combination produces nearly uniform sensitivity to the entire sky.

It is interesting to note that the blind spot of the southern site includes the richest concentration of matter in the nearby universe (out to 21 Mpc) [17]. It is therefore dangerous to suppose that the cosmic rays observed at the southern site are a fair representation of the full sky. The energy spectrum, the composition, and the clustering of arrival directions could all be different in the north and south. It is essential to make high-statistics measurements with identical detector types in both hemispheres.

Multipole moments are the natural way to characterize celestial anisotropy, provided full-sky coverage is available [18]. Each moment is the coefficient a_{lm} of a spherical harmonic function $Y_{lm}(\theta, \phi)$ in a series expansion of the celestial function. The lowest order harmonics (small l-values) govern the large-scale structure (dipole, quadrupole, octupole moments). The moments with large l-values determine the fine structure. Expansions out to $l \sim 30$ are ample for cosmic-ray measurements with angular resolution on the order of a degree. Magnetic dispersion may make it pointless to go beyond about $l = 10$. (At the highest energies where the magnetic dispersion is small, there will be too few arrival directions to determine many multipole moments.)

An example of an anisotropy fingerprint up to $l = 10$ is shown in Fig. 6. This heuristic example is based on an artificial assumption that the cosmic-ray sources are nearby infrared sources given in the point source catalogue PSCz [19]. The number of arrival directions from each source is taken in proportion to its apparent infrared luminosity. The magnetic dispersion is done using the source distance and a simple model of uniform nanogauss magnetic fields with coherence length of 1 Mpc. A total of 36 000 simulated arrival directions were used. They produced the multipole moments that are the fingerprint in Fig. 6. A simulation of an isotropic flux is also plotted in the figure for comparison. The anisotropy is manifest, and the fingerprint characterizes it. The fingerprint defines a function on the celestial sphere. Sampling arrival directions with that weighting function produces a scatter plot that is fully consistent with the original.

A rich celestial pattern like this is not possible for a realistic cosmic-ray observatory. Above the GZK energy threshold, it is possible to expect charged-particle astronomy. Particles are not deflected much by magnetic fields, and the sources cannot be far away. The nearby sources should be identifiable by the cosmic-ray arrival directions. Unfortunately, however, practical observatories cannot hope to achieve the exposure needed to get thousands of super-GZK arrival directions.

The 36 000 directions of Fig. 6 would be appropriate for a 5-year combined exposure of Auger South and Auger North at energies above 10^{19} eV, well below the GZK threshold. In that case, the majority of arrival directions will be cosmic rays that were produced billions of years ago, and which have been fully isotropized. The anisotropic foreground sources account for only about 1/60th of all arrival directions in that case. It is therefore relevant to ask if the fingerprint of Fig. 6 could be detected when it is diluted 59-to-1 by an isotropic distribution. As shown in Fig. 7, the answer is Yes. Any distribution of 36 000 arrival directions can be tested against the fingerprint of Fig. 6. The method is to compute its multipole moments (a'_{lm}) and then sum the products:

$$S \equiv \Sigma_{lm} \left(a_{lm} a'_{lm}\right) .$$

(This is like integrating the product of the two celestial functions. If they are similar, then the integral picks up systematically positive values rather than summing positive and negative values equally.) As shown in Fig. 7, simulations with 1/60th of the arrival directions being sampled from the distribution of Fig. 6 (and 59/60 isotropically) give a product sum that is distinctly non-zero. Simulations of complete

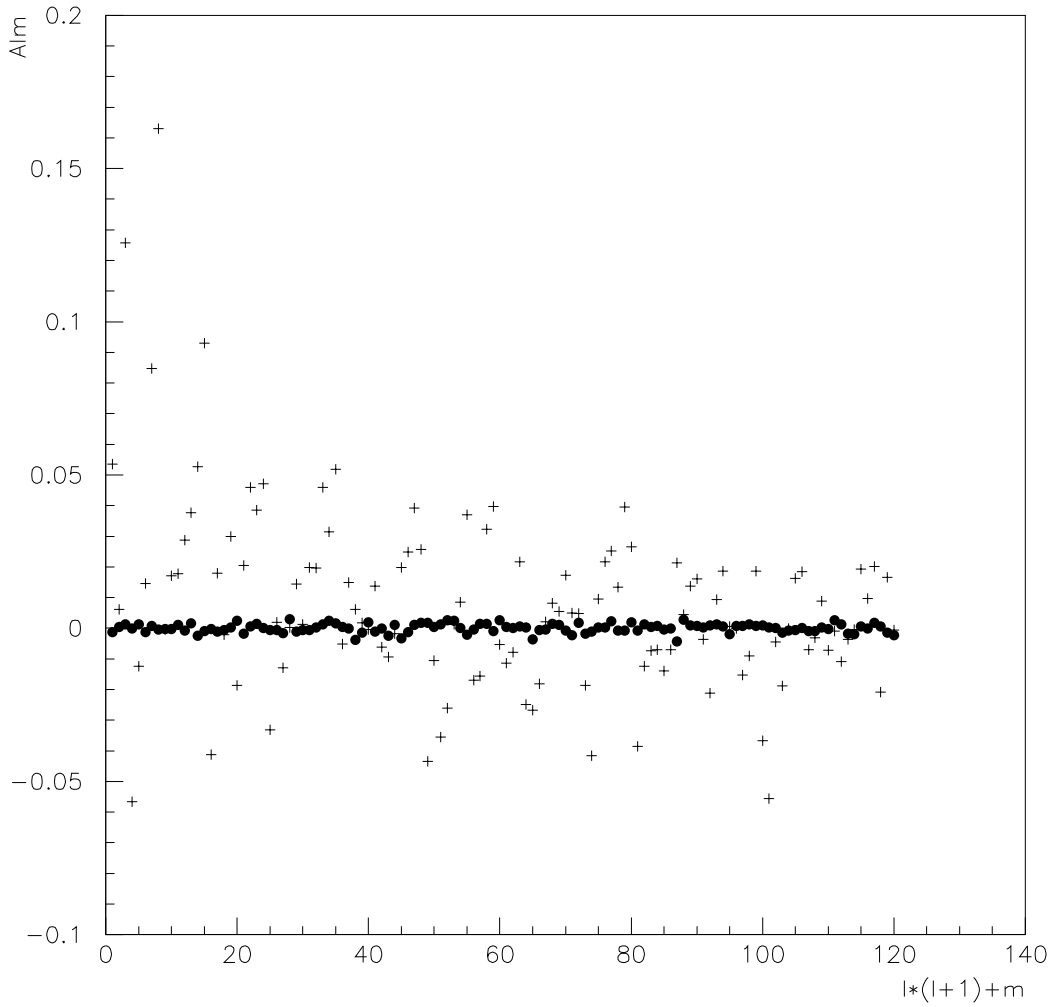

Fig. 6: An example of an anisotropy fingerprint. The 121 a_{lm} coefficients for $l \leq 10$ are plotted for a specific simple model of cosmic rays coming from nearby infrared sources. These are plotted with + signs. Also shown with • marks are results for an isotropic simulation with the same number of arrival directions (36 000). The set of a_{lm} values in the anisotropic case constitute a fingerprint of the anisotropy.

isotropy do not have a systematic offset from zero. The two distributions are almost disjoint, indicating that the foreground sources in this artificial model can be identified by their known fingerprint even in the presence of the dominant isotropic background.

Multipoles are not defined for a function on just part of a sphere. Without full-sky coverage, a cosmic-ray observatory cannot determine any of the a_{lm} coefficients. The powerful fingerprinting via multipole moments requires a full-sky observatory.

9 Summary

Properties of high-energy cosmic rays are inferred from measurements of their air showers. The cosmic-ray arrival direction, energy, and mass are determined indirectly. Combining different air-shower measurement techniques is important since each technique by itself is susceptible to systematic error as well as shower-by-shower uncertainties that result from shower development fluctuations and also fluctuations in the detector samplings.

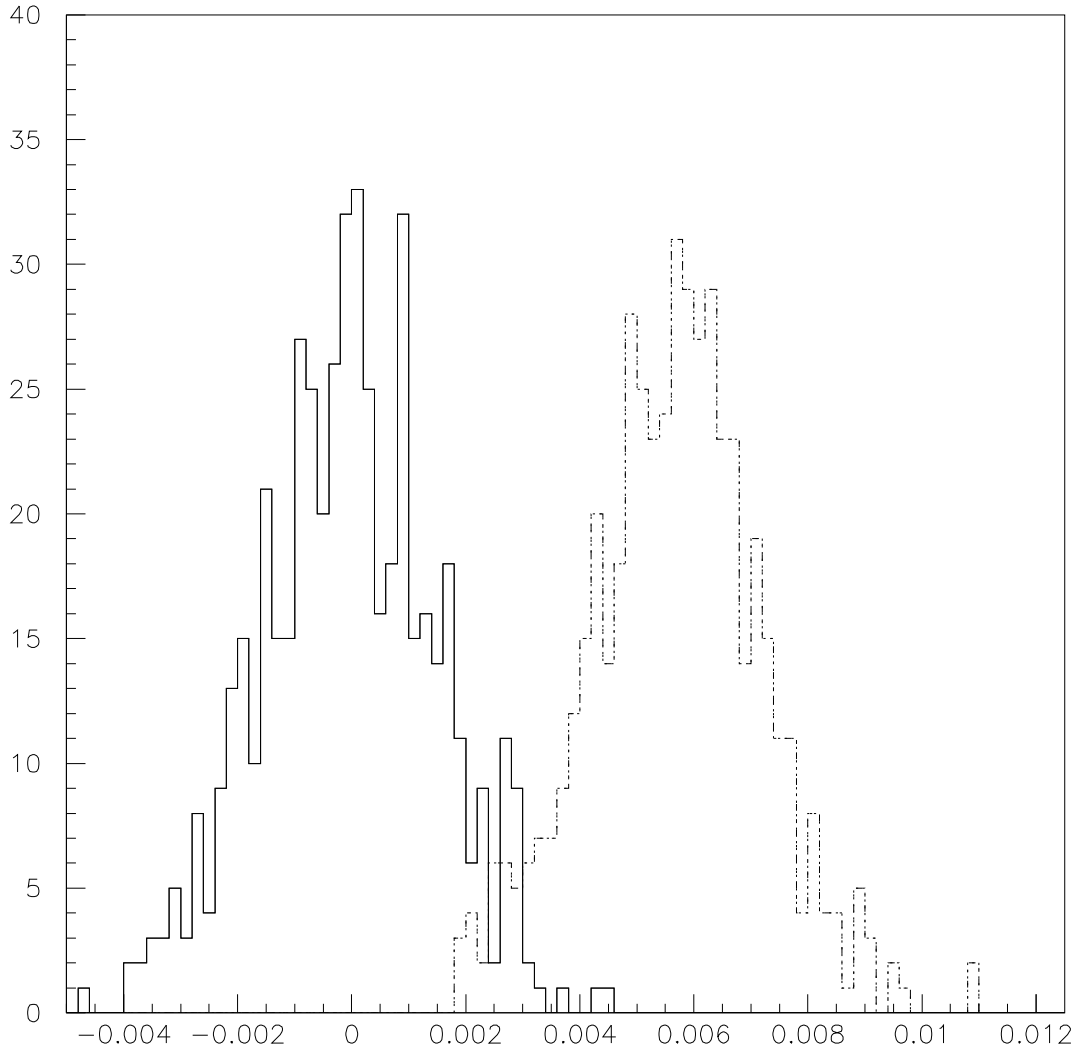

Fig. 7: Distinguishing the diluted anisotropy pattern. The left histogram (centred on zero) is derived from isotropic simulations, whereas, for the right histogram, each simulation has 1/60th of the arrival directions sampled from the PSCz anisotropy pattern used in Fig. 6. In each case, the variable represented in the histogram is the sum (over l and m) of the products of a_{lm} from the simulation times the a_{lm} of the PSCz anisotropy represented in Fig. 6.

The Auger Observatory, for example, combines a surface array of water Cherenkov detectors with telescopes that record air fluorescence produced by the secondary shower particles as they descend through the atmosphere. The hybrid air-shower measurements are crucial. They provide precision angular reconstructions for detector resolution studies and point source searches. They provide precision core locations for the study of SD-only geometric reconstructions. They determine the relationship of s_{1000} to electromagnetic energy at different zenith angles and energies. They provide $X_{\rm max}$ and the electromagnetic energy together with shower front curvature, lateral distribution steepness, and SD rise times for use in composition studies.

The surface detector operates on its own 90% of the time. It provides the high statistics needed for the high-energy end of the spectrum. It will measure the minuscule super-GZK flux. It has good sensitivity to EeV neutrinos. Its exposure is nearly uniform in right ascension due to the Earth's rotation. The declination dependence is easily calculated from the zenith angle acceptance. So the celestial exposure has a simple form which is easily calculated. Together with the high SD statistics, this results in sensitive anisotropy measurements.

Anisotropy analyses using data from only the southern site will be handicapped by a steep exposure gradient over half of the sky and a total blind spot in the quarter of the sky that is richest in nearby matter concentrations. The combination of Auger South with Auger North is needed for truly sensitive full-sky anisotropy analyses. A multipole moment 'fingerprint' could then characterize the celestial anisotropy in a small table of numbers.

References

[1] P. Auger *et al., Comptes Rendus* **206** (1938) 1721.

[2] M.A. Longair, *High Energy Astrophysics* (Cambridge University Press, 1992), vol. 1, pp. 118–122; W. Heitler, *The Quantum Theory of Radiation* (Dover, NY, 1984).

[3] K. Greisen, *Prog. Cosmic Rays* **3** (1956) 1.

[4] T. Gaisser and M. Hillas, *Proc. 15th ICRC*, Plovdiv, Bulgaria **8** (1977) 353.

[5] J.W. Elbert, Track reconstruction techniques and geometrical resolution in HiRes, *Proc. Tokyo Workshop on Techniques for the Study of Extremely High Energy Cosmic Rays*, M. Nagano [Ed.], (Institute for Cosmic Ray Research, University of Tokyo, 1993), p.158.

[6] http://www.auger.de/events/air-light-03/.

[7] K. Greisen, *Annu. Rev. Nucl. Sci* **10** (1960) 63.

[8] K. Kamata and J. Nishimura, *Prog. Theor. Phys.* (Kyoto) Suppl. 6 (1958) 93.

[9] J.W. Cronin, Particle discrimination using the FADC traces from the Auger Observatory surface detectors, Auger technical note GAP-2003-076 (2003).

[10] T.K. Gaisser *et al.,* A study of the chemical composition of cosmic rays around 10^{18} eV, *Comments Astrophys.* **17** (1993) 103–115.

[11] T. Abu-Zayyad *et al.,* Measurement of the cosmic ray spectrum and composition form 10^{17} to 10^{18} eV using a hybrid fluorescence technique, *Astrophys. J.* **557** (2001) 686.

[12] T. Abu-Zayyad *et al.,* A multi-component measurement of the cosmic ray composition between 10^{17} eV and 10^{18} eV, astro-ph/9911144.

[13] P. Billoir, *Comptes Rendus* **5** (2004) 495.

[14] L.D. Landau and I.Ya. Pomeranchuk, *Dokl. Akad. Nauk USSR* **92** (1953) 535; A.B. Migdal, *Phys. Rev.* **103** (1956) 1811.

[15] B. McBreen and C.J. Lambert, *Proc. 17th Int. Cosmic Ray Conf.* **6** (Paris, 1981) 70; T. Erber, *Rev. Mod. Phys.* **38** (1966) 626.

[16] K. Greisen, *Phys. Rev. Lett.* **16** (1966) 748; G.T. Zatsepin and V.A. Kuz'min, *JETP Lett.* **4** (1966) 78.

[17] J.W. Cronin, The highest-energy cosmic rays, Taup 2003 proceedings, astro-ph/0402487.

[18] P. Sommers, Cosmic ray anisotropy analysis with a full-sky observatory, *Astropart. Phys.*, **14** (2001) 271.

[19] http://www-astro.physics.ox.ac.uk/wjs/pscz.html